Original Article

MOLECULAR METABOLISM

PAR2 controls cholesterol homeostasis and lipid metabolism in nonalcoholic fatty liver disease

Rajashree Rana [1], Andrew M. Shearer [1,2], Elizabeth K. Fletcher [1], Nga Nguyen [1], Srijoy Guha [1], Daniel H. Cox [2], Manal Abdelmalek [3], Ying Wang [3], James D. Baleja [2], Lidija Covic [1,2], Athan Kuliopulos [1,2,*]

ABSTRACT

Objective: Increases in hepatic and plasma cholesterol occur in patients with nonalcoholic fatty liver disease (NAFLD), although the reason for this is not well understood. We investigated whether Protease-Activated Receptor 2 (PAR2) plays a role in cholesterol and lipid homeostasis in NAFLD.

Methods: Human liver biopsies (n = 108) were quantified for PAR2 expression from NAFLD cases randomly selected and stratified by liver fibrosis stage, the primary predictor for clinical outcomes, while controlling for age, gender, and BMI between fibrosis groups. Demographic data and laboratory studies on plasma samples were obtained within 6 months of liver biopsy. Wild-type and PAR2-KO (C57BL/6 F2rl1$^{-/-}$) mice were fed either normal or high fat diet for 16 weeks and plasma and liver assayed for lipids and soluble metabolites.

Results: Severity of NAFLD and plasma cholesterol levels significantly correlated with hepatocyte PAR2 expression in NAFLD patients. Conversely, PAR2 deficiency in mice resulted in reduced expression of key hepatic genes involved in cholesterol synthesis, a 50% drop in plasma and total liver cholesterol, and induced a reverse cholesterol transport system that culminated in 25% higher fecal bile acid output. PAR2-deficient mice exhibited enhanced fatty acid β-oxidation with a ketogenic shift and an unexpected increase in liver glycogenesis. Mechanistic studies identified G_i-Jnk1/2 as key downstream effectors of protease-activated PAR2 in the regulation of lipid and cholesterol homeostasis in liver.

Conclusions: These data indicate that PAR2 may be a new target for the suppression of plasma cholesterol and hepatic fat accumulation in NAFLD and related metabolic conditions.

Keywords Cholesterol; Energy metabolism; Fatty liver; Protease-activated receptor 2; NASH

1. INTRODUCTION

Excessive sugar and fat consumption can lead to a plethora of metabolic abnormalities including NAFLD [1]. The co-morbidities associated with NAFLD include hypercholesterolemia and dyslipidemia, obesity, insulin resistance, and metabolic syndrome. The progressive form of NAFLD, nonalcoholic steatohepatitis (NASH), is rapidly becoming the most common cause of chronic liver disease worldwide [2]. Increases in hepatic cholesterol also occur in patients with fatty liver disease and NASH for reasons that are not well understood [3]. Without any effective treatments to date, aside from lifestyle modification and weight-loss, NASH can often progress to liver fibrosis, cirrhosis, hepatocellular carcinoma, and liver transplantation with a combined 15-fold increase in liver-specific mortality compared to NAFLD.

The cell surface receptor PAR2 has recently been postulated to be involved in several critical pathways in NAFLD and NASH progression where it triggers inflammation, fibrosis, and hepatocellular necrosis [4]. Pharmacologic blockade of PAR2 effectively suppressed formation of reactive oxygen species (ROS) and lipotoxicity in hepatocytes [4], but the mechanistic basis for these effects was unknown. Unlike other G protein-coupled receptors, PAR2 is activated by cleavage of its N-terminal extracellular domain by trypsin-like or coagulation proteases [5,6] to generate a tethered ligand that induces a transmembrane signal to intracellular G_i and G_q pathways [7,8]. Tissue factor/Xa-initiated PAR2 activation was also found to stimulate diet-induced obesity and adipose inflammation in mouse models [9]. However, it has not been determined whether PAR2 is expressed in liver in NAFLD or NASH patients and whether hepatocyte PAR2 contributes to disease progression.

[1]Center for Hemostasis and Thrombosis Research, Tufts Medical Center, 800 Washington St, Boston, MA, 02111, USA [2]Tufts University School of Graduate Biomedical Sciences, Tufts University School of Medicine, Boston, MA, 02111, USA [3]Division of Gastroenterology and Hepatology, Duke University Medical Center, Durham, NC, 27710, USA

*Corresponding author. Center for Hemostasis and Thrombosis Research, Tufts Medical Center, 800 Washington St, Boston, MA, 02111, USA. E-mail: athan.kuliopulos@tufts.edu (A. Kuliopulos).

Abbreviations: NAFLD, nonalcoholic fatty liver disease; NASH, nonalcoholic steatohepatitis; PAR2, Protease-Activated Receptor 2; JNK, c-Jun N-terminal kinase; NAS, NAFLD activity score; Fib, Fibrosis

Received July 16, 2019 • Revision received August 16, 2019 • Accepted August 24, 2019 • Available online 28 August 2019

https://doi.org/10.1016/j.molmet.2019.08.019

Here, we found that PAR2 expression levels in hepatocytes significantly increase with disease progression in patients diagnosed with NAFLD and/or NASH. Patients with elevated levels of hepatic PAR2 had unexpectedly higher median plasma LDL cholesterol. Likewise, the livers of NAFLD mice had significantly increased *Par2* gene expression, which was highly correlated with plasma cholesterol levels. Conversely, PAR2-deficient mice had major drops in plasma cholesterol and liver cholesterol content in both high-fat and normal diets. PAR2-deficient animals exhibited attenuation in hepatic gene expression of *de novo* cholesterol synthesis enzymes, with upregulation of reverse cholesterol transport in liver and significantly enhanced fecal bile acid secretion. These changes were accompanied by suppression of *de novo* lipogenesis, enhancement of β-oxidation of fatty acids, a pronounced ketogenic shift, and glycogen cycling leading to production of anti-oxidant ascorbic acid. Mechanistic studies identified G_i-Jnk1/2, SREBP-1c, and AMPK as key downstream effectors of PAR2 signaling in liver. Together, these data indicate that blocking the activity of PAR2 may have broad salutary effects on cholesterol and lipid metabolism in NAFLD and NASH.

2. MATERIAL AND METHODS

2.1. Human studies

2.1.1. Patient selection and clinical parameters

We utilized the Duke University Health System (DUHS) NAFLD Clinical Database and Biorepository, an open enrolling database and biorepository which prospectively collected clinical data and biospecimens on patients who underwent a clinically indicated standard of care liver biopsy for evaluation of seronegative chronic liver disease. The DUHS NAFLD Clinical Database and Biorepository, this ancillary study, and informed consent procedures, were approved by the Duke Institutional Review Board (Duke University, Durham, NC). This study conformed to the principles set out in the WMA Declaration of Helsinki and the Department of Health and Human Services Belmont Report. Formalin-fixed paraffin embedded liver biopsy slides from patients with histologic diagnosis of NAFLD and NASH, non-NAFLD normal controls, and primary sclerosing cholangitis (PSC) acquired from April 2006 through July 2018 were retrieved for immunohistochemistry staining for PAR2. NAFLD was defined as the presence of >5% hepatic steatosis on liver biopsy and absence of histologic and serologic evidence for other chronic liver disease in a patient with risk factors for metabolic syndrome. NAFLD cases were randomly selected and stratified by liver fibrosis stage: F0-1, F2, F3-4 (F4 included both compensated and uncompensated cirrhosis), the primary predictor for clinical outcomes, while controlling for age (±5 years), gender, and BMI (±3 points) between fibrosis groups. Demographic data (e.g. BMI, age, sex, race, comorbid conditions) and laboratory studies on plasma samples (e.g. total cholesterol, LDL and HDL cholesterol, triglycerides, liver alanine aminotransferase (ALT), and aspartate aminotransferase (AST)) were obtained within 6 months of liver biopsy.

2.1.2. Human liver biopsies and PAR2 immunohistochemistry

Each liver biopsy had been previously processed for routine histology, graded, and staged for the histologic features for NAFLD/NASH according to the NASH Clinical Research Network Grading and Staging System [10]. Deparaffinized liver biopsies were either stained for collagen deposition with Massons trichrome or subjected to heat-mediated antigen-retrieval (10 mM citrate, 0.05% Tween 20, pH 6.0) and stained with the monoclonal PAR2 SAM11 Ab (Santa Cruz SC-13504) and secondary-Ab (goat anti-mouse) conjugated to HRP (Dako P0447) and developed with 3,3-diaminobenzidine (DAB).

2.2. Animal models and diet

All animal experiments were performed in accordance with institutional guidelines of the NIH and approved by the Tufts Institutional Animal Care and Use Committee. Wild-type male C57BL/6 mice (6–8 weeks; originally purchased from Charles River Laboratories) and PAR2-KO (C57BL/6 F2rl1$^{-/-}$) mice [7] were bred in our facility. Mice were housed 4 per cage, with a 12 h light/dark cycle, 7AM on (Z = 0), 7PM off, in climate-controlled rooms in the certified and accredited Division of Laboratory Animal Medicine (DLAM) at Tufts University. Mice were fed either a normal diet (Envigo/Harlan 2918: protein 24% kcal, fat 18% kcal, carbohydrate 58% kcal) or a 60% high fat diet (Research Diets D12492: protein 20% kcal, fat 60% kcal, carbohydrate 20% kcal) for 16 weeks and permitted food and water consumption *ad libitum*. Body weight and food consumption were recorded weekly. At the end of the experimental period, whole blood was collected into heparin (10 U/mL) anti-coagulant at time Z+4 to +6 (non-fasting) by cardiac puncture and plasma isolated. Animals were euthanized with CO_2 following anesthesia. Livers were isolated and weighed, and a portion was fixed in formaldehyde for histopathological analyses, with the remaining tissue flash frozen and stored at −80 °C to be subsequently used for biochemical, gene expression, and metabolomic analyses.

2.3. Biochemical assays of cholesterol, triglyceride, free fatty acids, and fecal bile acids

Plasma and hepatic lipid content of mice fed normal or 60% high fat diets were assayed using biochemical assays. Livers frozen in liquid N_2 were ground into a fine powder with a mortar and pestle and lipids extracted and resolubilized in aqueous media and quantified using kits for total cholesterol (Cell Biolabs: STA-384), triglycerides (Cayman Chemical: 10010303) and free fatty acid (abcam: ab65341) using the manufacturer's protocols. Fecal pellets were collected over a 2 week period from individually housed mice fed 60% high fat diet and dried at room temperature for 72 h. Dried fecal pellets were homogenized in 75% ethanol and incubated at 50 °C for 2 h. Extracts were then centrifuged at 250*g* for 5 min. The supernatants were collected and diluted with 1X PBS (1:4) and used for bile acid measurements using the Mouse Total Bile Acids Kit from Crystal Chem (Catalog #80470) as before [11].

2.4. Quantitative real-time PCR

Total RNA was extracted from frozen liver homogenates using the RNeasy Mini kit (Qiagen) and cDNA synthesized using reverse transcriptase. Real time quantitative PCR of various gene targets was

conducted using SYBR Green Master Mix (Roche) and a 40-thermocycling protocol. ΔΔCT data are represented as relative-fold changes in mRNA normalized to β-actin.

Gene Targets Table: F = Forward primer, R = Reverse primer.

Gene	Mouse Sequence
F2rl F	5′-CTTGCACCGGGACGCA-3′
F2rl R	5′-AAAGCCTGGTTCTACCGGAAC-3′
Hmgcs1 F	5′-GTCTGATCCCCTTTGGTGGCT-3′
Hmgcs1 R	5′-AAGAGCTGTGTGAAGGACAGAGA-3′
Hmgcr F	5′-ACGTGGTGTGTCTATTCGCC-3′
Hmgcr R	5′-AGCAAGCTCCCATCACCAAG-3′
Cyp7A1 F	5′-AGCAACTAAACAACCTGCCAGTACTA-3′
Cyp7A1 R	5′-GTCCGGATATTCAAGGATGCA-3′
Abcb11 F	5′-CAGGGAGGCCAAAGGTGAGC-3′
Abcb11 R	5′-ATGGTGGCAGGGAATGAAAAGTAG-3′
Abcb4 F	5′-CCTCCGACAAGAAATGGGCT-3′
Abcb4 R	5′-CACTGATTTTGGAGACGTCATCTG-3′
Abcg5 F	5′-CCTGCTGAGGCGAGTAACAA-3′
Abcg5 R	5′-GGACGCGGAGAAGGTAGAAA-3′
Abcg8 F	5′-CTACCAGGTGGACATCGCCTC-3′
Abcg8 R	5′-TAGATTTCGGATGCCCAGCTC-3′
Npc1 F	5′-GGGTCACCTACGTGGCATTT-3′
Npc1 R	5′-ACACAAAGTACCGCCTTCTGT-3′
Ldlr F	5′-CCAATCGACTCACGGGTTCA-3′
Ldlr R	5′-TCACACCAGTTCACCCCTCT-3′
Srb1 (Scarb1) F	5′-GGCTGCTGTTTGCTGCG-3′
Srb1 (Scarb1) R	5′-GCTGCTTGATGAGGGAGGG-3′
Lipe F	5′-GCTGGGCTGTCAAGCACTGT-3′
Lipe R	5′-GTAACTGGGTAGGCTGCCAT-3′
Pnpla2 F	5′-TTCACCATCCGCTTGTTGGAG-3′
Pnpla2 R	5′-AGATGGTCACCCAATTTCCTC-3′
Acaca (Acc1) F	5′-CCTGAAGACCTTAAAGCCAATGC-3′
Acaca (Acc1) R	5′-CCAGCCCACACTGCTTGTA-3′
Fasn F	5′-GTTCGACGCCTCCTTTTTTG-3′
Fasn R	5′-GCGTCTCGGGATCTCTGCTA-3′
Scd1 F	5′-CAGGTTTCCAAGCGCAGTTC-3′
Scd1 R	5′-TTCACCTTCTCTCGTTCATTTCC-3′
Acsl1 F	5′-AGCTATCCTGGACGACTTGTTGA-3′
Acsl1 R	5′-AGATCTTGATGGTGGCGTACAGT-3′
Acaa2 F	5′-GAACGCCTCGGGGGTG-3′
Acaa2 R	5′-CCAGGGGCGTGAAGTTATGT-3′
Hmgcs2 F	5′-ACCACCAACGCCTGTTATGG-3′
Hmgcs2 R	5′-GCATAGCGACCATCCCAGTA-3′
Hmgcl F	5′-TGTACCCACCCCAGTGAAGA-3′
Hmgcl R	5′-GAGTGGTCAGCCATCTGTGG-3′
Bdh1 F	5′-CTCCGAAGAGCCAAAGGTCG-3′
Bdh1 R	5′-CGAGAAAGCCTCGATCCCAA-3′
Sref1 F	5′-AGTACCTTTGGTTGTGGACACAGA-3′
Sref1 R	5′-GCACTTCGTAGGGTCAGGTTCT-3′
Ppargc1a F	5′-AGCACGAAAGGCTCAAGAGG-3′
Ppargc1a R	5′-CGGCGCTCTTCAATTGCTTT-3′
Ppargc1b F	5′-GGCCTTGTGTCAAGGTGGAT-3′
Ppargc1b R	5′-AGGTGCTTATGCAGTTCCGT-3′
Ppara F	5′-GGGAACTTAGAGGAGAGCCAAG-3′
Ppara R	5′-TGACAACGTCTTGTTCCCGA-3′
Fgf21 F	5′-AGATCAGGGAGGATGGAACA-3′
Fgf21 R	5′-TCAAAGTGAGGCGATCCATA-3′
Actb F	5′-TTCTTTGCAGCTCCTTCGTTGCCG-3′
Actb R	5′-TGGATGGCTACGTACATGGCTGGG-3′

2.5. Mouse liver histopathological analyses

Blinded histopathological analyses of liver sections were performed as previously described [4]. Briefly, mouse livers were fixed in 10% neutral buffered formalin at 4 °C overnight and embedded in paraffin wax. Liver tissues were sectioned (5 μm), stained with hematoxylin & eosin, and observed with a Nikon Eclipse 80i microscope connected to a Spot 7.4 Slider camera with 10 randomly chosen 200X fields. Each mouse liver section was scored for steatosis, inflammation, and ballooning and the composite NAFLD Activity Score (NAS) recorded using pre-established guidelines for human liver from the Nonalcoholic Steatohepatitis Clinical Research Network (NASH CRN) Pathology Committee [10].

2.6. Extraction of soluble metabolites from liver and plasma

Liver tissue was ground to a fine powder in liquid nitrogen, transferred to Eppendorf tubes and snap frozen at −80 °C. Soluble metabolites were extracted from liver as previously described [12]. Briefly, 50 mg of ground liver tissue was homogenized in a methanol-water (methanol 4 mL/g, water 8.5 mL/g) mixture. The homogenates were then transferred to glass vials and chloroform (8 mL/g) and water (4 mL/g) added sequentially. Homogenates were vortexed for 60 s and placed on ice for 10 min. The samples were then centrifuged for 5 min at 2000*g* at 4 °C to remove precipitated protein and tissue debris and to separate the polar and non-polar layers. The top layer was removed and dried in a speed-vac. Alternatively, 200 μL of plasma was extracted with 200 μL methanol, placed at −20 °C for 20 min and centrifuged at 14,000*g* for 20 min to obtain soluble plasma metabolites in the supernatant. The dried metabolites were dissolved in 50 mM phosphate buffer pH 7.2 (99.8% D_2O) with 200 μM 4,4-dimethyl-4-silapentane-1-sulfonic acid (DSS) internal standard.

2.7. ^{1}H-NMR spectroscopy

^{1}H NMR spectra of aqueous liver and plasma metabolites from WT and PAR2-KO mice were acquired at 25 °C on a Bruker 600 MHz spectrometer. A one-dimensional (1D) NOESYPRESAT pulse sequence was applied with D_2O as the frequency lock. For each sample, spectra were acquired with 67 K data points and 128 scans over a spectral width of 14.02 ppm. Water suppression was achieved during the relaxation delay of 1 s and mixing time of 100 ms. The free induction decay was processed with Chenomx software (version 6.3, Alberta, Canada) for Fourier transformation. All spectra were phase and baseline-corrected and referenced to the DSS peak at 0.00 ppm. A line-broadening factor of 0.5 Hz was applied to all spectra. The concentrations of the metabolites were determined by comparing the integral of the known reference signal (DSS) with the signal derived from a library containing chemical shifts and peak multiplicities for all of the resonances of the respective standard compounds. Resultant data sets of quantified metabolites were exported to Microsoft Excel format.

2.8. Cell culture

HuH7 hepatocytes (human male donor) were authenticated by STR profiling and were free of mycoplasma contamination. HuH7 cells were maintained in low glucose Dulbecco's-modified eagle's medium (DMEM) (Corning Cellgro), supplemented with 10% fetal bovine serum (FBS) (Atlanta Biologicals) and 1% penicillin-streptomycin (Invitrogen). The cells were maintained at 37 °C in a humidified atmosphere containing 5% CO_2. For inhibitor treatments, HuH7 cells were serum starved in basal DMEM (without FBS) for 4 h and pretreated with the Jnk1/2 inhibitor SP600125 (Sigma Aldrich) for 45 min or pertussis

toxin for 16 h before being stimulated with trypsin (10 nM). Stock concentrations of SP600125 were made in 20% DMSO. The final concentration of DMSO added to the HuH7 cells was maintained at 0.2% and was included in the vehicle control. HuH7 hepatocytes were grown to 50–60% confluence and transfected with duplex siRNA targeted against PAR2 (5′-AGGAAGAAGCCUUA UUGGU-3′) or control siRNA (5′-CGTACGCGGAATAC TTCGA-3′) using oligofectamine reagent (Invitrogen) in opti-MEM medium as before [4,7]. Following transfection for 48 h, cells were starved for 4 h and PAR2 stimulated with trypsin (Sigma) for 15 min and lysates collected for western blot.

2.9. Western blot analysis

Whole cell lysates from human HuH7 hepatocytes were prepared in RIPA lysis buffer (50 mM Tris-HCl, pH 7.4, 1% NP-40, 0.5% sodium deoxycholate, 0.1% SDS, 150 mM NaCl, 2 mM EDTA and 50 mM sodium fluoride) in the presence of protease and phosphatase inhibitors (Halt Protease and Phosphatase Inhibitor Cocktail, Sigma). For subcellular-fractionation and separation of cytoplasmic and nuclear proteins, cells were briefly washed with cold PBS and gently scraped with cytoplasmic protein extraction buffer (20 mM HEPES, 10 mM potassium chloride, 5 mM magnesium chloride, 1 mM EDTA, 10% glycerol and 0.2% NP-40). The cell lysates were centrifuged for 10 min at 775*g* and the supernatant collected for cytoplasmic proteins. Nuclear pellets were washed once with the cytoplasmic protein extraction buffer and lysed in RIPA buffer. Equal amounts of protein (10–100 μg) were resolved by 10% SDS-PAGE for western analysis. The primary antibodies for human phospho-Jnk (Thr183/Tyr185) (#4671S), total Jnk (#9252S), phospho AMPKα (Thr172) (#2531), total AMPKα (#2532S), and β-tubulin (#2146S) were purchased from Cell Signaling. The SREBP1/SREBP-1c antibody used was purchased either from Santa Cruz (sc-365513) for mouse liver lysates or Novus Biologicals (NB100-60545) for HuH7 cell lysates. The Lamin A antibody was purchased from Santa Cruz (sc-20680).

2.10. Statistical analysis

Statistical analyses were performed using GraphPad Prism 6 or R. Results are expressed as mean ± SEM or median ± quartiles. A logistic regression model of PAR2 staining as the dependent variable and fibrosis stage (adjusted for sex and diabetes) as the independent variable was used to analyze the human liver biopsy data. LDL cholesterol levels of NAFLD/NASH subjects with low PAR2 versus high PAR2 staining of liver biopsies was analyzed by Pearson's chi-squared test (Mood's median test) for statistical significance. Mouse and hepatocyte data were analyzed by ANOVA followed by Tukey's multiple comparisons tests for experiments having more than two cohorts. For statistical analyses between two cohorts, 2-tailed unpaired t-test with $\alpha = 0.05$, thus $P < 0.05$ was considered significant.

3. RESULTS

3.1. PAR2 expression levels increase with disease progression in the livers of patients with NAFLD

We conducted a cross-sectional study of liver specimens and clinical data from 93 NAFLD patients and 15 controls with normal liver biopsies to examine the relationship, if any, between hepatic PAR2 expression and progression of NAFLD. Subjects were selected with both milder NAFLD fibrosis (Fib) stage 0–2 (n = 50), and severe Fib stage 3–4 (n = 43). NAFLD patients ranged in age from 29 to 75 and were 44% male with a mean BMI of 35.6 kg/m^2 (Table 1). Typical NAFLD risk factors included obesity (78%) and diabetes mellitus (55%). The mean NAFLD activity score (NAS) score was 4.4 ± 1.4 and the mean fibrosis score was 2.3 ± 1.2. The Fib 3–4 cohort had significantly higher AST levels (P = 0.0005) and lower HDL cholesterol (P = 0.026), but no significant differences in total cholesterol, LDL cholesterol, or triglycerides as compared to the Fib 0–2 cohort (Table S1). The 15 control subjects had a NAS score of 0 with normal liver parenchyma (Figure 1A), were generally younger, non-obese, and 67% were male (Table 1). All 108 liver biopsies were stained for PAR2 protein expression, which was scored for intensity in a blinded manner. PAR2 protein expression was low in control livers (Figure 1A) and progressively increased in subjects with mild NAFLD fibrosis (Figure 1C) and NAFLD with higher stages of fibrosis (Figure 1B). The PAR2 protein staining was particularly evident in the periphery/plasma membrane of hepatocytes in severe NAFLD fibrosis (Figure 1D). Logistic regression analysis across the cohorts (adjusting for sex and diabetes) revealed a highly significant relationship (P = 0.01) between high PAR2 expression and increasing severity of NAFLD fibrosis (Figure 1E). Unexpectedly, the high PAR2-expressing NAFLD cohort had significantly elevated (+21 mg/dL, $P < 0.05$) median plasma LDL cholesterol (Figure 1F) as compared to the low PAR2-expressing cohort, with non-significant numerical increases in total plasma cholesterol, liver enzymes AST and ALT, and proportion of males (Table S2).

3.2. PAR2 promotes hypercholesterolemia in mice

To determine whether PAR2 expression in liver plays a causal role in NAFLD progression and cholesterol homeostasis, wild-type (WT) and PAR2-deficient (KO) mice were fed a standard high fat diet (HFD: 60%-kcal fat, 20%-kcal carbohydrates, 20%-kcal protein) for 16 weeks to induce NAFLD. At the end of the experiment, PAR2-KO mice had a striking 46% decrease ($P < 0.001$) in plasma cholesterol compared to WT mice (Figure 2A). As steady-state cholesterol levels and overall flux are regulated by liver [13], we assessed PAR2 expression levels in liver tissue from WT mice. Mean hepatic *Par2* expression significantly increased by 2-fold in WT mice fed HFD compared to mice fed normal chow diet (ND) (Figure 2B). There was a highly significant linear correlation ($R^2 = 0.61$, $P < 0.0001$) between hepatic *Par2* expression and total plasma cholesterol (Figure 2B) with a 1.6-fold increase ($P < 0.001$) in mean cholesterol levels in WT mice on HFD versus normal diet.

Table 1 – Baseline characteristics of patients (n = 108) with liver biopsies.

Characteristic	NAFLD/NASH patients (n = 93)	Control patients (n = 15)
Age, y	53 ± 9	45 ± 15
Range	29–75	22–74
Male, n	41 (44%)	10 (67%)
BMI, kg/m^2	35.6 ± 7.0	26.3 ± 3.9
Range	24.2–62.7	21.0–34.6
Obesity[a]	73 (78%)	2 (13%)
Diabetes mellitus	51 (55%)	4 (27%)
Race, n		
White	83 (89%)	12 (80%)
Black	9 (10%)	3 (20%)
American Indian	1 (1%)	0 (0%)
NAS[b] (0–8)	4.4 ± 1.4	0
Steatosis (0–3)	1.8 ± 0.8	0
Inflammation (0–3)	1.3 ± 0.6	0
Ballooning (0–2)	1.3 ± 0.6	0
Fibrosis Score (0–4)	2.3 ± 1.2	0.2 ± 0.8

Data represent mean ± SD where indicated.
[a] Subjects with BMI ≥30 kg/m^2.
[b] NAS is the NAFLD activity score as previously defined [10].

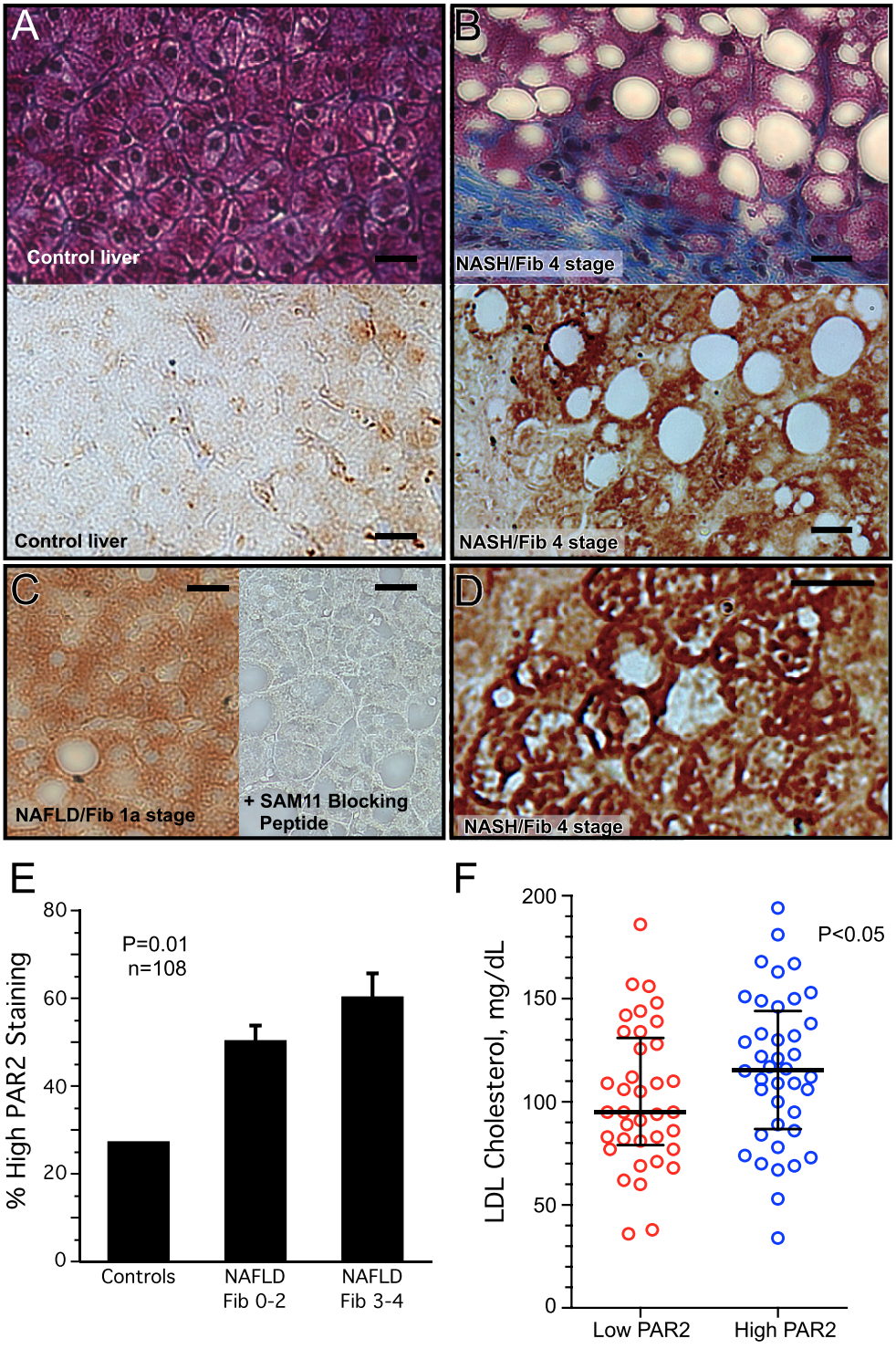

Figure 1: PAR2 expression is enhanced in the livers of patients with NAFLD and NASH and is associated with high LDL cholesterol. Liver biopsies were obtained from 93 subjects with the diagnosis of NAFLD/NASH with fibrosis scores ranging from 0 to 4, along with 15 control subjects with normal liver biopsies. (A) Photomicrographs (400x) of control liver biopsy and (B) fibrosis stage 4 NASH subject biopsy stained with Masson's trichrome to show blue collagen matrix deposition and macrovesicular steatosis (white empty spaces) in top panels. PAR2 staining (brown-SAM11 Ab) of control liver and fibrosis stage 4 NASH patient shown below. (C) PAR2 staining of NAFLD patient with mild stage 1a fibrosis (left panel), also in the presence of the SAM11 blocking peptide, SLIGKVDGTSVTG (right panel) (400x). (D) PAR2 staining of fibrosis stage 4 NASH patient at 800× magnification depicting strong PAR2 staining at periphery/plasma membrane of individual hepatocytes. (E) PAR2 staining of liver biopsies was scored as high or low in a blinded manner in control subjects (n = 15), NAFLD/NASH subjects with fibrosis score of 0–2 (n = 50), and NASH subjects with severe fibrosis scores of 3–4 (n = 43). A logistic regression model of PAR2 staining as the dependent variable and NAFLD fibrosis stage (adjusted for sex and diabetes) as the independent variable was used to analyze the data. (F) LDL cholesterol levels of NAFLD/NASH subjects with low PAR2 versus high PAR2 staining of liver biopsies. Data was analyzed by Pearson's chi-squared test (Mood's median test) for statistical significance with medians and interquartile ranges shown. Black bar = 25 μm.

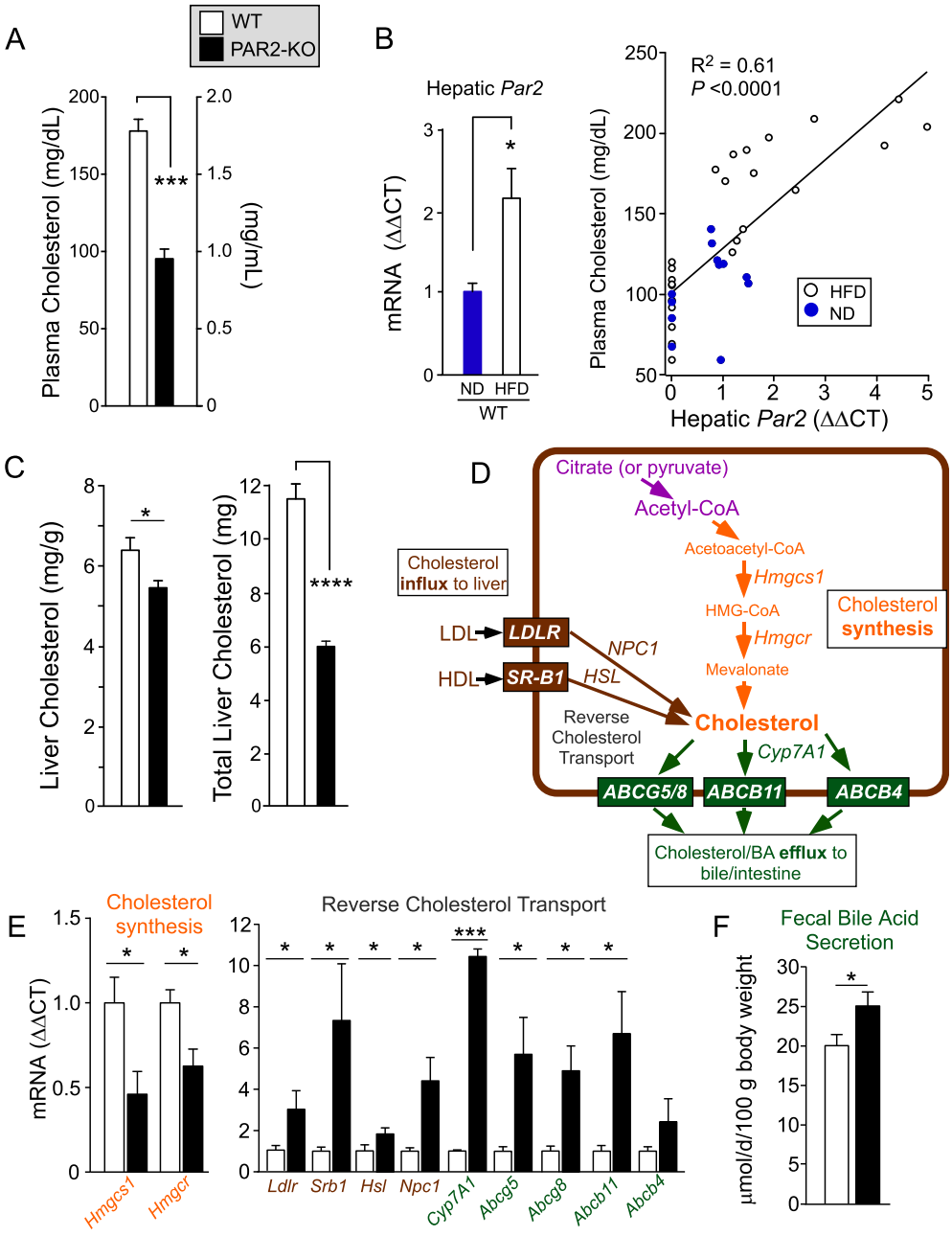

Figure 2: PAR2 deficiency suppresses hypercholesterolemia and enhances reverse cholesterol transport in liver in HFD-fed mice. Male C57BL/6 wild type (WT-open bars) and PAR2-KO (KO-black bars) mice were fed 60% high fat diet (HFD, n = 10–14) for 16 weeks. (A) At the 16 week endpoint, plasma was obtained from non-fasted mice at Z+4 time point and assayed for total cholesterol. (B) Quantitative PCR (ΔΔCT) of hepatic *Par2* mRNA from mice fed normal diet (ND) or HFD for 16 weeks, normalized to *β-actin*. Plasma cholesterol significantly correlated with hepatic *Par2* expression from mice fed both ND and HFD. Linear regression analysis was performed and least-squares lines, R^2 values and P values for the slope are shown. (C) Livers from mice in A were harvested and weighed at the 16 week endpoint and assayed for mg cholesterol per g of liver tissue and total liver cholesterol content. (D) Hepatic transporters and enzymes controlling cholesterol flux and synthesis pathways affected by PAR2-deficiency in livers of mice fed a HFD diet for 16 weeks. (E) Quantitative PCR (ΔΔCT) of mRNA from mouse liver (normalized to *β-actin* mRNA) for *Hmgcs1* (*3-hydroxy-3-methylglutaryl-Coenzyme A synthase 1*), *Hmgcr (3-hydroxy-3-methylglutaryl-Coenzyme A reductase)*, *Hsl (Hormone Sensitive Lipase)*, *Npc1* (*NPC intracellular cholesterol transporter 1*), *Abcg5* (*ATP-binding cassette, sub-family G member 5*), *Abcg8* (*ATP-binding cassette, sub-family G member 8*), *Abcb11* (*ATP-binding cassette, sub-family B, member 11*), *Abcb4* (*ATP-binding cassette, sub-family B, member 4*), *Ldlr (low-density lipoprotein receptor)*, *Srb1* (*scavenger receptor class B, member 1*) in WT and PAR2-KO mice fed HFD for 16 weeks. (F) Mean fecal bile acid content from HFD-fed mice in A during a two-week collection period. All data are represented as mean ± SEM; Unpaired 2-tailed T-tests were performed,*P < 0.05, ***P < 0.001, ****P < 0.0001.

3.3. PAR2 deficiency suppresses cholesterol synthesis and stimulates reverse cholesterol transport in liver

Given the increase in *Par2* expression in livers from mice fed HFD and the major suppressive effect of PAR2-deficiency on plasma cholesterol, hepatic cholesterol levels were assessed. PAR2-deficiency gave a 15% reduction in hepatic cholesterol concentration (P < 0.05) and 47% reduction in total liver cholesterol burden (P < 0.0001) compared to WT (Figure 2C). In mice fed a normal non-NAFLD diet for 16 weeks, PAR2-deficiency also led to a significant decrease in both plasma and liver cholesterol compared to wild-type

animals without significantly affecting liver weight, body weight or daily food intake (Figures S1A–F). Cholesterol biosynthesis from citrate or pyruvate precursors is initiated by the cytoplasmic enzyme hydroxymethylglutaryl-CoA synthase (HMGCS1) that forms HMG-CoA (Figure 2D). The next step is catalyzed by the rate-determining 3-hydroxy-3-methylglutaryl-coenzyme A reductase (HMGCR), the expression of which is increased by 2–3 fold in NAFLD and NASH patients [3]. As shown in Figure 2E, expression of *Hmgcs1* and *Hmgcr* were significantly down-regulated by 2.2-fold and 1.6-fold respectively in PAR2-KO livers compared to WT.

Cholesterol synthesized in extrahepatic tissues is esterified to cholesterol ester, packaged into HDL particles, and released into circulation where it is eventually removed by the scavenger receptor class B, member 1 (SR-B1) on the surface of hepatocytes and other cells [14]. After internalization by SR-B1, hormone-sensitive lipase (HSL) hydrolyzes the cholesterol esters to free cholesterol. In addition, the LDL receptor (LDLR) is crucial for the uptake of cholesterol from plasma LDL particles into the liver. NPC intracellular cholesterol transporter 1 (NPC1) moves internalized cholesterol derived from LDL into post-lysosomal compartments in hepatocytes and other cells [15]. Expression of these genes controlling cholesterol influx from blood into liver was examined. As shown in Figure 2E, *Ldlr* and *Srb1* were significantly upregulated by 3-fold and 7.3-fold, respectively, in PAR2-KO mouse livers compared to WT after 16 weeks of HFD. Likewise, the downstream *Npc1* and *Hsl* genes were significantly upregulated by 4.5-fold and 2-fold, respectively, in the PAR2-KO livers.

Cholesterol 7α-hydroxylase (Cyp7A1) is the rate-limiting enzyme in the primary pathway of bile acid synthesis. As shown in Figure 2E, *Cyp7A1* expression was significantly upregulated by 10-fold ($P < 0.001$) in the PAR2-KO mice. To complete the process of reverse cholesterol transport in hepatocytes, an array of cholesterol/sterol and bile transporters (ATP-binding cassette) Abcb5/8, Abcb11 (BSEP), and Abcb4 pump cholesterol and bile acids from the hepatocyte into the bile canaliculi (Figure 2D). The gene expression of all four of these cholesterol efflux transporters was induced by 2.3- to 6.7-fold in the PAR2-KO mouse livers compared to WT mice after 16 weeks of HFD. Mouse feces collected over a two-week period during HFD feeding showed a significant 25% increase ($P < 0.05$) in bile acid content in the PAR2-KO mice compared to WT (Figure 2F). Together, these data indicate that PAR2 is involved in regulating the process of reverse cholesterol transport in mouse liver, which results in enhanced plasma cholesterol and reduced bile acid secretion.

3.4. PAR2 promotes diet-induced liver hypertriglyceridemia and NAFLD

Unlike the effects seen with plasma cholesterol, PAR2-deficient mice had no change in plasma triglycerides (Figure 3A) or HFD food consumption over the 16 week time period relative to WT (Figure S1G). Contrary to the plasma triglyceride levels, the PAR2-KO mice had a highly significant 50% drop in mean hepatic triglycerides ($P < 0.01$) and a trend ($P = 0.07$) towards 26% lower free fatty acids in liver (Figure 3B). The PAR2-KO mice had 22% lower liver/body weight (Figure 3C) and much less fatty liver disease by histology with a striking 3.5-fold drop in NAFLD activity score (NAS) score ($P < 0.01$) when compared to WT mice (Figure 3D). All components of the NAS score including steatosis, lobular inflammation, and ballooning hepatocyte injury were significantly lower in PAR2-KO mice as compared to WT; however, liver inflammation was minimal with a mean score of only 0.5 in the WT mice fed HFD for 16 weeks. We examined the gene expression of key enzymes of *de novo* lipogenesis (DNL), which produce fatty acids and triglycerides starting from citrate or pyruvate precursors (Figure 3E). As shown in Figure 3F, PAR2-KO mouse livers had attenuated levels of *acetyl-CoA carboxylase 1 (Acc1)* (1.8-fold lower, $P < 0.05$) and *fatty acid synthase (Fas)* (3.1-fold lower, $P < 0.01$) and nearly complete suppression of *stearoyl CoA desaturase 1 (Scd1)* (36-fold lower, $P < 0.001$) expression as compared to WT mice on HFD. Together, these data are consistent with the observed drop in free fatty acid and triglyceride content in the livers of PAR2-deficient mice.

3.5. PAR2-KO mice exhibit enhanced β-oxidation, ketogenesis, and TCA cycling

We determined whether the PAR2-deficient mice had increased fatty acid catabolism in their livers. To initiate hepatic β-oxidation, triglycerides first undergo lipolysis by lipases including adipose triglyceride lipase (ATGL) and HSL, which release free fatty acids (Figure 4A). Liberated fatty acids are transported to the mitochondria and undergo β-oxidation to produce energy as ATP and acetyl-CoA. Acyl-CoA synthetase (ACS) is a crucial enzyme that provides substrate for both lipogenesis and oxidation. Acetyl-Coenzyme A acyltransferase 2 (ACAA2) catalyzes the last step of mitochondrial β-oxidation to release acetyl-CoA that then enters the tricarboxylic acid cycle (TCA cycle). As shown in Figure 4B, the mean hepatic expression of *Atgl* increased by 5-fold ($P < 0.05$), *Hsl* by 2-fold (Figure 2E), *Acs* by 3-fold ($P < 0.001$), and *Acaa2* by 4-fold ($P < 0.01$) in the PAR2-KO mice compared to WT mice fed HFD.

To examine the effects of PAR2 on overall liver metabolism, we conducted NMR-metabolomics on liver lysates from WT and PAR2-KO mice after 16 weeks of HFD. Acetyl-CoA produced by β-oxidation is the key intermediary metabolite serving both as a substrate for the TCA cycle as well as for ketone synthesis (Figure 4A). The primary site for ketogenesis is hepatic mitochondria. Excess acetyl-CoA produced by β-oxidation is condensed to acetoacetyl-CoA, which is converted to HMG-CoA by the mitochondrial enzyme HMG-CoA synthase (HMGCS2). HMG-CoA lyase (HMGCL) then converts HMG-CoA to acetoacetate, which is converted to 3-hydroxybutyrate by beta-hydroxybutyrate dehydrogenase (BDH1). As shown in Figure 4C, the expression of the key enzymes of ketogenesis - *Hmgcs2*, *Hmgcl*, and *Bdh1* - were all significantly increased by 3-5-fold ($P < 0.05$) in PAR2-KO mice compared to WT mice fed HFD. In addition to directly promoting mitochondrial fatty acid oxidation and ketogenesis, HMGCS2 regulates the expression of fibroblast growth factor 21 (FGF21) in hepatocytes [16], a signaling molecule induced in ketotic states [17,18]. Indeed, a significant ($P < 0.01$), 5-fold increase in hepatic expression of *Fgf21* was observed in the PAR2-KO mice compared to WT. Consistent with these ketogenic transcriptional effects, there was a major increase in β-hydroxybutyrate concentrations in plasma (3.8-fold, $P < 0.001$) and liver (2-fold, $P < 0.001$) in the PAR2-KO mice fed HFD (Figure 4D). Furthermore, there was an increase in TCA intermediates including citrate (1.7-fold), succinate (1.7-fold), fumarate (1.7-fold), and malate (3.8-fold) in the PAR2-KO mice (Figure 4E) consistent with excess acetyl-CoA from β-oxidation being directed towards the TCA cycle. The TCA cycle intermediate α-KG, is also a precursor for glutamate and glutamine synthesis; accordingly, hepatic concentrations of glutamate and glutamine were significantly increased by 1.5–1.7-fold in PAR2-KO mice relative to WT mice (Figure 4F). With the observed increase in TCA-flux, we also documented a decrease in NAD+ and an increase in NADH concentrations which gave a significant drop in the NAD+/NADH ratio by 3-fold ($P < 0.05$) in the PAR2-KO mice compared to WT mice on HFD (Figure 4F).

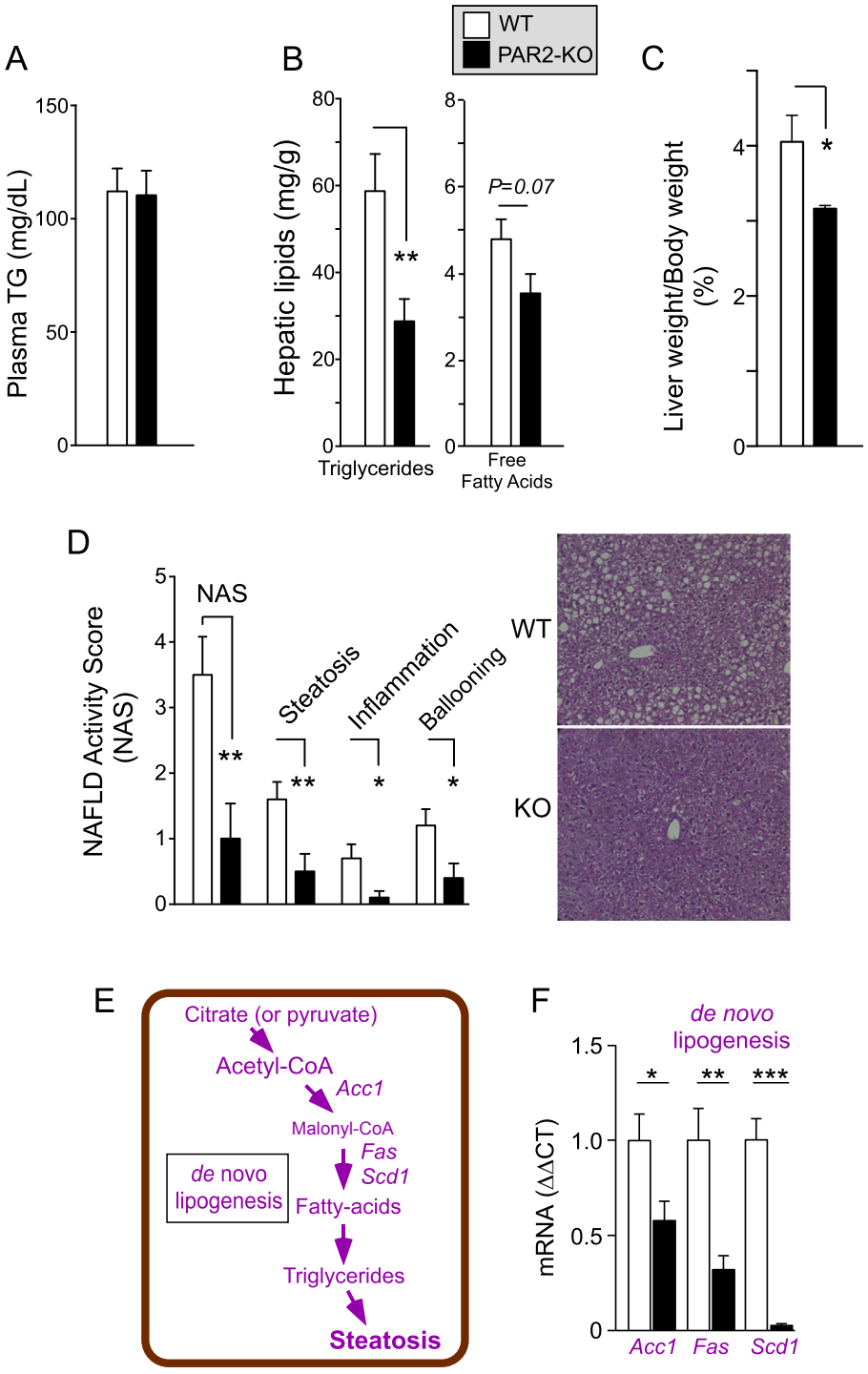

Figure 3: PAR2 deficiency significantly reduces NAS score in NAFLD and expression of genes involved in *de novo* lipogenesis in mice. Male C57BL/6 wild type and PAR2-KO mice were fed 60% high fat diet (HFD, n = 10–14) for 16 weeks. (A) At the 16 week endpoint, plasma was obtained from non-fasted mice (Z+4) and assayed for triglycerides. (B) Livers from mice in A were harvested at the 16 week endpoint and assayed for triglycerides and free fatty acids. (C) Mean %Liver/Body weight at 16 weeks. (D) NAFLD-Activity Score (NAS) comprising steatosis, inflammation, and ballooning was determined in a blinded manner from hematoxylin and eosin (H&E) stained sections of mouse liver from WT and PAR2-KO mice fed HFD for 16 weeks. (E) Hepatic enzymes controlling *de novo* lipogenesis. (F) Quantitative PCR (ΔΔCT) mRNA from mouse liver (normalized to *β-actin* mRNA) for *Acc1* (*acetyl-CoA carboxylase 1*), *Fas* (*fatty-acid synthase*) and *Scd1* (*stearoyl-Coenzyme A desaturase 1*). Data represent mean ± SEM from 4 to 5 mice per gene analyzed. Unpaired 2-tailed T-tests were performed; *P < 0.05, **P < 0.01, ***P < 0.001.

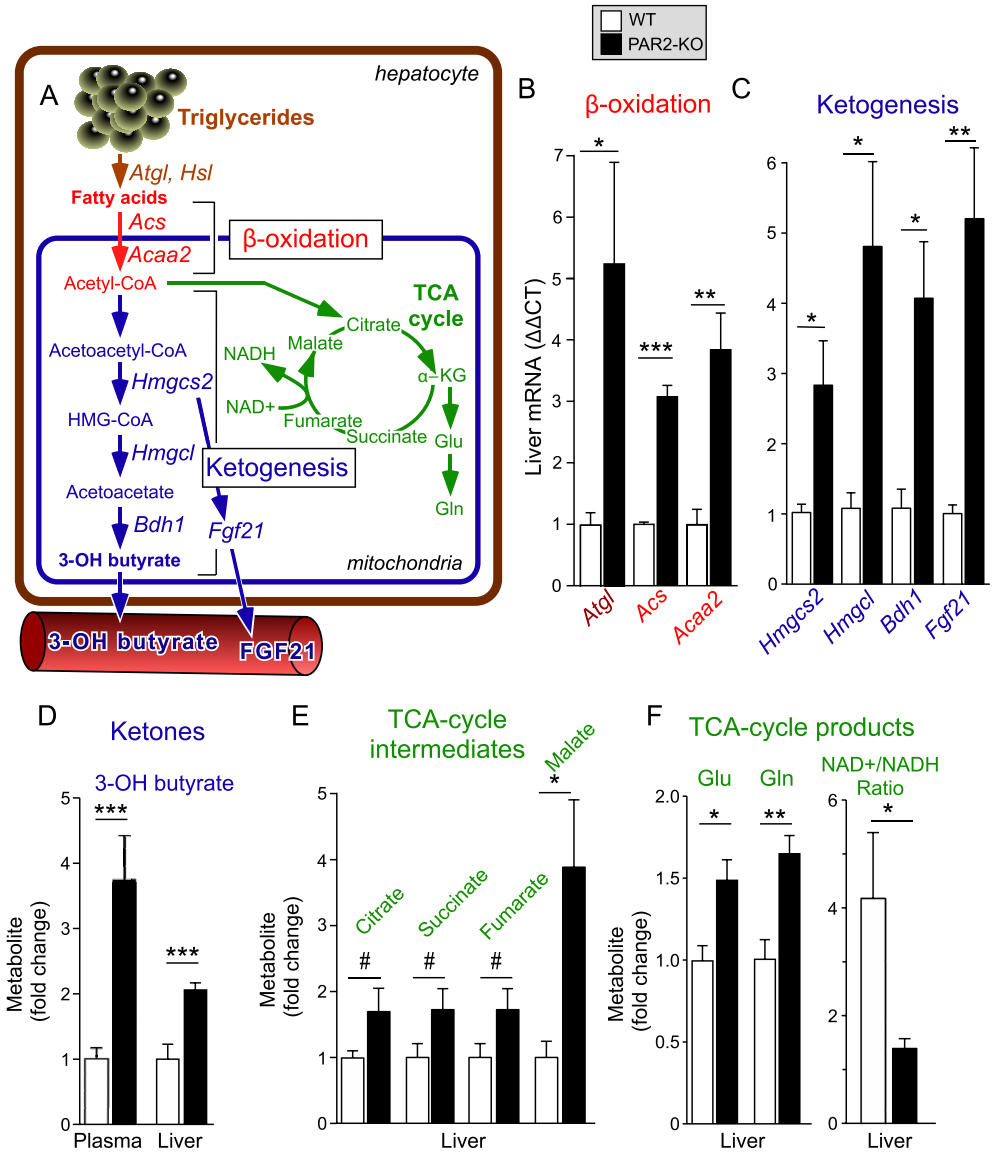

Figure 4: PAR2 deficiency significantly upregulates hepatic genes involved in fatty acid β-oxidation and induces a ketogenic shift in HFD-fed mice. (A) Metabolic pathways controlling fatty acid breakdown and ketone synthesis affected by PAR2-deficiency in livers of mice fed a HFD diet for 16 weeks. (B–C) Quantitative PCR (ΔΔCT) of mRNA from mouse liver (normalized to *β-actin* mRNA): *Atgl (Adipose triglyceride lipase)*, *Acs (long chain fatty acyl-CoA ligase or synthetase)*, *Acaa2 (acetyl-Coenzyme A acyltransferase 2)*, *Hmgcs2* (*3-hydroxy-3-methylglutaryl-Coenzyme A synthase 2)*, *Hmgcl* (*3-hydroxy-3-methylglutaryl-Coenzyme A lyase*) and *Bdh1* (*3-hydroxybutyrate dehydrogenase, type 1*), *Fgf21 (fibroblast growth factor 21)* in WT and PAR2-KO mice fed HFD for 16 weeks. Data for *Hsl* shown in Figure 2E. (D–F) Plasma and/or liver metabolites in WT vs PAR2-KO mice fed HFD for 16 weeks was quantified by NMR-metabolomic methods, Glu = glutamate, Gln = glutamine. Data represent mean ± SEM from 3 to 10 mice per gene and 6–9 mice per metabolite analyzed; unpaired 2-tailed T-tests were performed, *$P < 0.05$, **$P < 0.01$, ***$P < 0.001$, $^{\#}P = 0.1$.

3.6. PAR2-deficient mice have elevated glycogen and ascorbate synthesis in liver

The PAR2-KO mice had a 12% drop ($P < 0.05$) in mean glucose levels (Figure 5A) with 156 ± 13 mg/dL in KO mice vs 179 ± 10 mg/dL in WT mice. There was a non-significant, 17% drop in blood pyruvate in PAR2-KO compared to WT mice in this non-diabetic, HFD model. Elevated citrate levels from enhanced fatty acid β-oxidation and TCA cycling can inhibit phosphofructokinase 1 (PFK1) and suppress glycolysis (Figure 5C) in a Randle-type mechanism. If operating in the PAR2-KO mice, this scenario would predict that glycolysis would be inhibited, leading to a decrease in pyruvate and an increase in glucose in liver. Indeed, as shown in Figure 5A, there was a highly significant, 14% drop in pyruvate ($P < 0.01$) and a non-significant, 21% increase in liver glucose indicating decreased hepatic glycolysis. Notably, there was a significant increase in glycogen synthesis metabolites including UDP-glucose (2.2-fold, $P < 0.001$), glycogen itself (1.9-fold, $P < 0.05$), and ascorbate (1.7-fold, $P < 0.05$), which is synthesized from UDP-glucose in mice and other non-primate animals (Figure 5B). These data show that excess hepatic glucose is shunted into a glycogenesis pathway of storage rather than glycolysis in the PAR2-deficient mice compared to WT under conditions of HFD.

3.7. PAR2 activates JNK-SREBP-1c pathways in liver and hepatocytes

Jnk1/2 has been proposed to play a key role in the development of fatty liver disease [19] and can regulate liver cholesterol homeostasis by

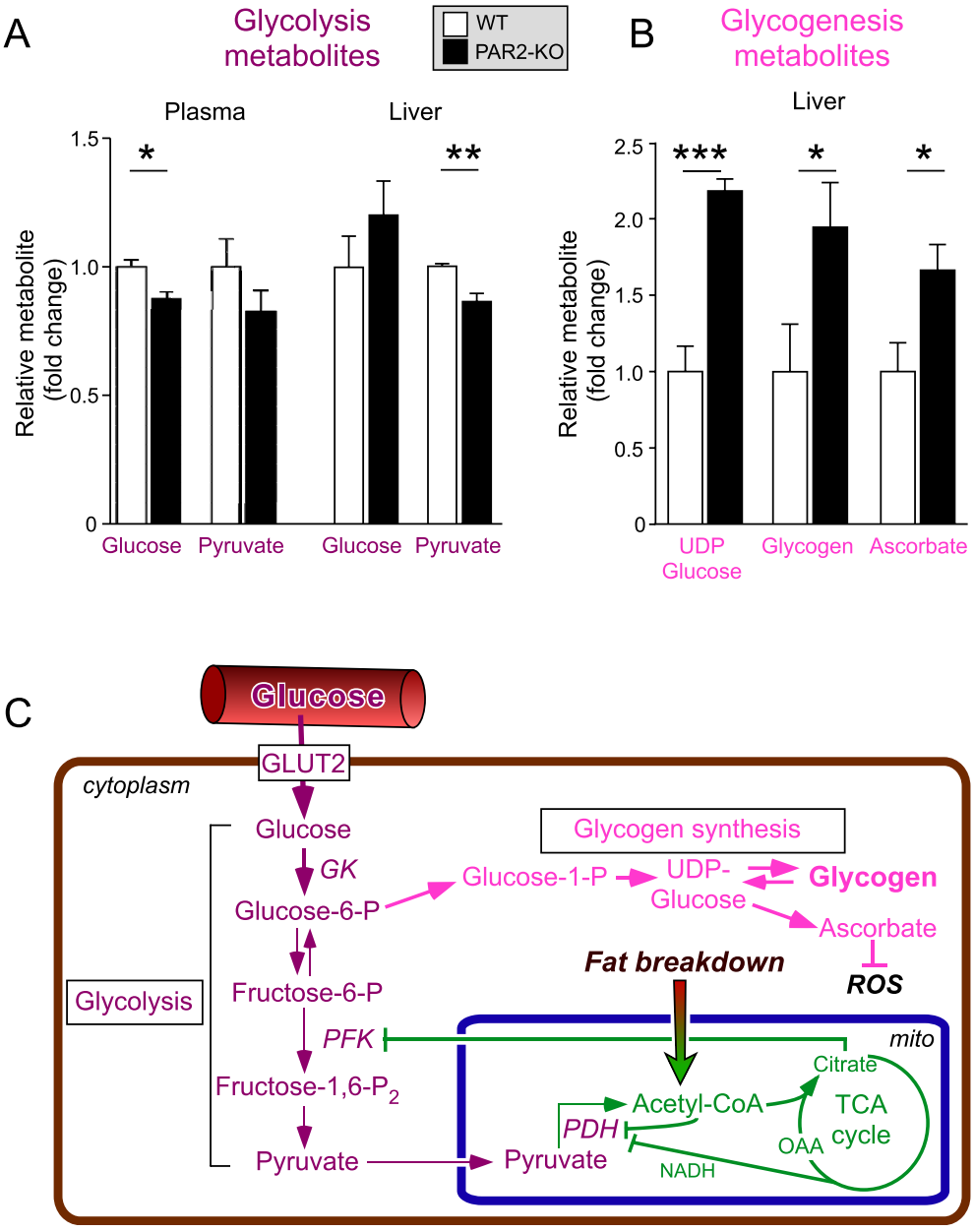

Figure 5: PAR2 deficiency induces glycogenesis and ascorbate production in livers of HFD-fed mice. (A—B) Plasma and liver glycolysis and glycogenesis metabolites in WT vs PAR2-KO mice fed HFD for 16 weeks were quantified by NMR-metabolomic methods. (C) Glycolysis and glycogenesis pathways and regulation in the livers of PAR2-deficient mice. Data represent mean ± SEM from 6 to 9 mice per metabolite analyzed; unpaired 2-tailed T-tests were performed, *P < 0.05, **P < 0.01, ***P < 0.001.

suppressing expression of the rate limiting bile acid synthesis enzyme Cyp7A1 [20,21]. Sterol regulatory element-binding protein-1c (SREBP-1c) is the major lipogenic transcription factor [22] that activates genes of fatty acid, triglyceride, and cholesterol/sterol synthesis, and suppresses AMPK-driven catabolism. To gain insight into the key signaling pathways regulated by PAR2, we examined the hepatic activity of Jnk1/2 and AMPK and the active cleaved form of SREBP-1c in the liver of WT and PAR2-KO mice fed ND and HFD. As shown in Figure 6A, hepatic phosphorylation of Jnk1/2 (Thr183/Tyr185) was increased by 5-fold ($P < 0.001$) in WT mice fed HFD diet relative to ND. PAR2-KO mice were completely protected against this diet-induced Jnk1/2 activation with significantly lower (6.9-fold, $P < 0.001$) phospho-Jnk1/2 levels. Furthermore, the active proteolytic 65 kDa fragment of SREBP-1c was increased by 3.3-fold in the livers of WT mice fed HFD as compared to ND, whereas the PAR2-KO mice were completely protected from the increase in active SREBP-1c under conditions of HFD (Figure 6A). There were no significant differences in the levels of the active cleaved form of SREBP-2 (64 kDa) in the livers of the WT and KO mice on HFD diet (Figure S2A).

SREBP-1c (anabolism) and AMPK activity (catabolism) exhibit an inverse correlation [23]. Accordingly, PAR2-KO mice fed HFD had higher (3.5-fold, $P < 0.001$) phosphorylation of AMPK (Thr172) when compared to WT mice, with no significant differences in phospho-AMPK status in the WT mice fed HFD vs ND (Figure 6A). Furthermore, the hepatic mRNA expression of *Srebp1c* was significantly decreased (3.4-fold, $P < 0.01$) in PAR2-KO mice relative to WT mice

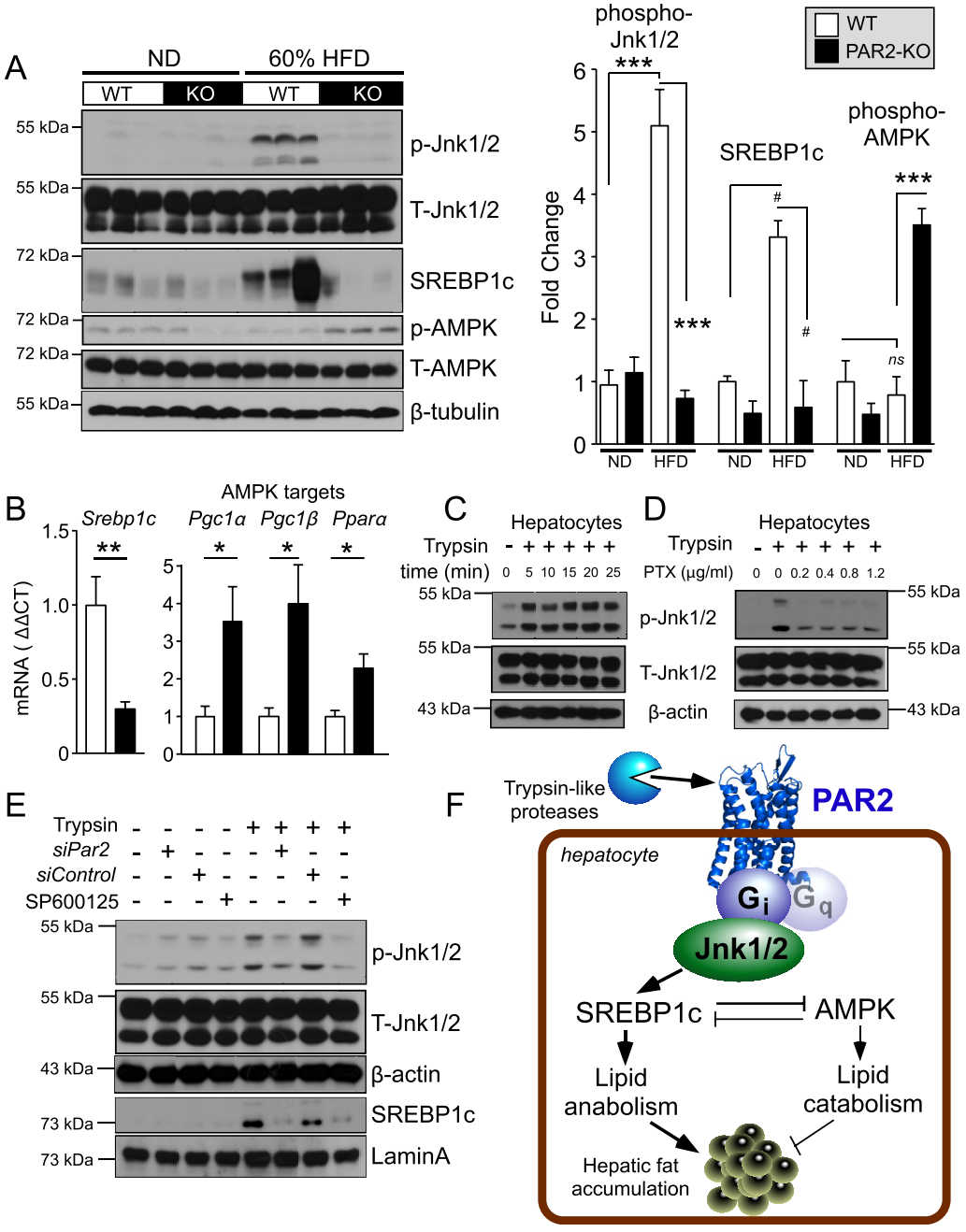

Figure 6: PAR2-Gi activates JNK-SREBP-1c pathways that induce hepatic lipid accumulation in HFD-fed mice. (A) Western blots of liver lysates from WT and PAR2-KO mice fed either normal chow diet (ND) or high fat diet (HFD) for 16 weeks. Densitometric quantification of western blots on left for Phospho (P)-Jnk1/2 normalized to total (T)-Jnk1/2, active 65 kDa proteolytic fragment of SREBP-1c normalized to β-tubulin, and Phospho (P)-AMPK normalized to total-AMPK. (B) Quantitative PCR (ΔΔCT) of mRNA from mouse liver (n = 5) normalized to *β-actin* mRNA of *Srebp1c* and AMPK targets: *Pgc1α* (*peroxisome proliferative activated receptor, gamma, coactivator 1 alpha*), *Pgc1β* (*peroxisome proliferative activated receptor, gamma, coactivator 1 beta*) and *Pparα* (*peroxisome proliferator activated receptor alpha*). (C–D) Trypsin (10 nM) induces phospho-Jnk1/2 signaling in HuH7 hepatoma cells, which is suppressed by the Gi inhibitor, pertussis toxin (PTX); 15 min time-point used in D. (E) Par2 siRNA (500 nM) knockdown inhibits trypsin-induced phosphorylation of Jnk1/2 (15 min) in HuH7 cells. Trypsin induces nuclear translocation of SREBP-1c, which is inhibited by *siPAR2* and by the Jnk1/2 inhibitor SP600125. β-actin and Lamin A were used as loading controls for whole cell and nuclear lysate western blots, respectively. (F) Mechanism of PAR2-Gi regulation of lipid metabolism in hepatocytes by activating Jnk1/2 and SREBP-1c pathways. One-way ANOVA followed by Tukey's post-hoc test (A) or unpaired 2-tailed T-test (B) was performed, *P $<$ 0.05, **P $<$ 0.01, ***P $<$ 0.001, #P = 0.06.

on HFD (Figure 6B). Likewise, the expression of the AMPK targets *Pgc1α*, *Pgc1β*, and *Pparα* were all significantly elevated by 2-4-fold in PAR2-KO compared to WT mice fed HFD (Figure 6B).

To gain insight into the potential mechanism by which PAR2 might regulate Jnk1/2-SREBP-1c signaling, we performed mechanistic studies using the HuH7 hepatocyte cell line. Treatment of HuH7 cells with the PAR2 agonist trypsin caused sustained phosphorylation of Jnk1/2 for at least 25 min (Figure 6C). Pretreatment of the HuH7 cells with the G_i-inhibitor pertussis toxin resulted in attenuation of trypsin-induced phosphorylation of Jnk1/2 (Figure 6D). Silencing HuH7

hepatocyte PAR2 with a validated *siPar2* [4] suppressed the trypsin-induced phosphorylation of Jnk1/2 and the appearance of active nuclear SREBP-1c compared to *siControl* RNA, which was also blocked by treatment with the Jnk1/2 inhibitor SP600125 (Figure 6E). In addition to G_i, PAR2 is also a G_q-coupled receptor [24,25]. Blockade of G_q with the potent YM-254890 compound had no effect on the ability of PAR2 to activate Jnk1/2 in HuH7 cells (Figure S2B). These data are consistent with the mechanism depicted in Figure 6G, namely that activated PAR2 induces robust Jnk1/2 signaling through a G_i-coupled pathway. Phosphorylated Jnk1/2 in turn activates SREBP-1c to induce hepatic lipid anabolism and inhibition of AMPK activity leading to increased lipid synthesis and fat deposition in liver.

4. DISCUSSION

Steady-state cholesterol levels in blood are maintained by a balance of dietary uptake, *de novo* synthesis, and excretion as bile steroids by reverse-cholesterol transport from the liver into the intestines [13]. Increases in hepatic cholesterol synthesis and suppression of reverse cholesterol transport occur in patients with NAFLD and NASH although the reason for this is not well understood [3]. The present study made the unanticipated discovery that the cell surface protease-activated receptor PAR2 is expressed at significantly higher levels in the hepatocytes of patients with more severe NALFD/NASH fibrosis and correlates with higher levels of plasma LDL cholesterol. *Par2* expression was also significantly increased in the livers of NAFLD mice fed a HFD and was highly correlated with plasma cholesterol levels. Conversely, PAR2-deficient mice had significant 40—60% attenuation in hepatic gene expression of *de novo* cholesterol synthesis enzymes HMG-CoA reductase (*Hmgcr*) and synthase (*Hmgcs1*), with 50% drops in plasma cholesterol and total liver cholesterol content.

PAR2-null animals also had upregulation of genes controlling all steps of reverse cholesterol transport in liver with significantly enhanced fecal bile acid secretion compared to WT mice. Expression of genes involved in hepatic cholesterol uptake from HDL and LDL lipoproteins, including *Srb1*, *Hsl*, *Ldlr*, and *Npc1*, were significantly elevated in the PAR2-deficient mice fed HFD. The SR-B1 scavenger receptor for HDL cholesterol is most abundantly expressed in liver [26] and was upregulated by 7-fold in the PAR2-deficient mice. Transcription of *Srb1* is controlled by SREBP-1/cAMP, with cAMP regulating SF-1 activation of the *Srb1* promoter [14]. After binding of HDL to the SR-B1 receptor, hormone-sensitive lipase (HSL) hydrolyzes the HDL-cholesterol ester cargo into free cholesterol, and it becomes available for further catabolism [14]. HSL is also regulated by cAMP/PKA, and *Hsl* gene expression was upregulated by 2-fold in the PAR2-deficient mice. Consistent with these transcriptional effects, the PAR2 receptor is strongly coupled to G_i [7,8], which suppresses cAMP pathways through inhibition of adenylyl cyclase.

The other major receptor for cholesterol-containing lipoproteins, namely the LDL receptor, is decreased in the liver of subjects with NAFLD and NASH [3]. We discovered that *Ldlr* expression was significantly upregulated in the livers of the PAR2-KO mice compared to WT mice. Conversely, in mice lacking the LDL receptor, PAR2 knockout had no effect on plasma cholesterol levels [27], consistent with the notion that the presence of the LDL receptor is essential for operation of efficient reverse cholesterol transport in liver. After endocytosis of the LDL receptor, the bound LDL is internalized to the lysosomes where cholesterol is exported into the cell by the NPC1 cholesterol transporter [15], which is regulated by PKA-cAMP-CREB. *Npc1* gene expression was enhanced 4-fold in the PAR2-KO livers under conditions of HFD. Despite upregulation of the *Srb1*, *Hdlr*, *Hsl*, and *Npc1* genes, steady-state cholesterol levels were actually decreased in the PAR2-KO livers providing evidence that the internalized cholesterol was efficiently pumped out of the liver into the intestines as bile steroids [28]. Indeed, the PAR2-deficient mice had significantly increased bile steroids in their feces. Accordingly, there was a 10-fold upregulation in expression of the rate-limiting bile steroid synthesis enzyme *Cyp7A1* and 2.3—6.7-fold increases in the major cholesterol/bile steroid transporters *Abcg5*, *Abcg8*, *Abcb11*, and *Abcb4*. ABCB11 (BSEP) is responsible for the rate limiting step of bile acid transport, increased biliary flow and secretion of monovalent bile acids from hepatocytes into the canaliculi [13]. ABCB11 is expressed in an inverse correlation with histopathological progression of NAFLD in humans [29]. Hepatic ABCG8 levels are also downregulated in NASH patients [3].

De novo lipogenesis of fatty acids is an important metabolic pathway in subjects with NAFLD contributing to approximately 25% of hepatic triglycerides with 15% from diet [30]. Despite no changes in HFD food intake or plasma triglyceride levels, PAR2-deficient mice exhibited a 50% drop in hepatic triglycerides and 26% drop in hepatic free fatty acids with a major protection against development of hepatic steatosis. Acetyl-CoA carboxylase 1 (ACC1) and fatty acid synthase (FAS) are the key enzymes catalyzing *de novo* lipogenesis and expression of their genes were significantly reduced by 2—3 fold in the PAR2-KO mice. Deletion of ACC1 or ACC2 generally results in lowered liver triglycerides [1]. However, liver-specific ACC1/2-KO or pharmacologic inhibition causes a decrease in polyunsaturated fatty acids (PUFAs), which induce SREBP-1c and VLDL secretion resulting in increased systemic triglyceride levels [31]. In the PAR2-KO mice, plasma triglycerides were unaffected, and both gene transcripts and protein levels of active SREBP-1c were decreased, indicating that PAR2 controls SREBP-1c via a pathway distinct from ACC/PUFA-mediated regulation. Interestingly, gene expression of stearoyl coenzyme A desaturase 1 (SCD1) was almost completely suppressed in the livers of PAR2-KO relative to WT mice on HFD. SCD1 catalyzes the rate-limiting step in the formation of mono-unsaturated fatty acid (MUFAs), and overexpression of SCD1 has been linked to hypertriglyceridemia and Familial Combined Hyperlipidemia (FCHL) in humans [32]. SCD1 antisense therapy protected mice against NAFLD on HFD and a SCD1 inhibitor, aramchol, decreased hepatic lipid content in humans with HIV-associated lipodystrophy/NAFLD, pointing to SCD1 as a potential therapeutic target in the broader NAFLD population [1].

PAR2-KO mice also exhibited enhanced β-oxidation of fatty acids, leading to a marked ketogenic shift under conditions of HFD. Ketogenesis occurs when acetyl-CoA produced by β-oxidation exceeds the ability of the TCA cycle to produce citrate and ketones synthesized in the hepatic mitochondria are instead utilized by extrahepatic tissues as an energy source [33]. We discovered that the gene expression of key enzymes of triglyceride hydrolysis (ATGL, HSL), fatty acid β-oxidation (ACS, ACAA2), and ketogenesis (HMGCS2, HMGCL, BDH1) were all significantly elevated by 3—5 fold in the livers of PAR2-KO mice. Expression of *Ppara*, the master regulator of fatty acid β-oxidation [34—36], and PPARα-coactivators *Pgc1a* and *Pgc1b* [37], which protect against diet-induced steatosis, were all found to be upregulated in the livers of the PAR2-KO mice. PPARα and HMGCS2 are also known to increase the expression of the hepatokine FGF21 [16—18], and we noted a major increase in the expression of FGF21 in the livers of the PAR2-KO mice. This was accompanied by a highly significant increase in the β-hydroxybutyrate ketone end product both in liver (3.5-fold) and plasma (2-fold). Reduced lipogenesis may also account for increased β-oxidation through a mechanism that does not involve changes in expression of oxidative genes. This occurs because

malonyl-coA is an inhibitor for CPT, the rate-limiting enzyme in mitochondrial β-oxidation of fatty acids [38]. Abundant β-oxidation product acetyl-CoA is also consumed by the TCA cycle. The livers of the PAR2-KO mice exhibited heightened TCA flux as evident by an increase in the concentrations of the TCA cycle intermediates citrate, succinate, fumarate, and malate, with a major 3-fold decrease in the NAD+/NADH redox ratio. The TCA cycle intermediate α-KG is a precursor for glutamate and glutamine synthesis and hepatic concentrations of these amino acids were significantly increased in the livers of PAR2-KO mice fed HFD.

As PAR2 is expressed by many tissues and cell types and a conventional whole-body knockout was used, it is unclear how much of the mouse phenotype on liver fatty acid metabolism is mediated only at the level of the hepatocyte and how much is due to loss of PAR2 at other sites of expression such as adipose tissue, macrophages, or the endothelium. However, significant suppressive effects of the whole-body PAR2 knockout on plasma and liver cholesterol were also observed in lean mice under normal diet conditions with normal livers (non-steatotic, non-inflammatory), consistent with the notion that PAR2 on adipocytes or inflammatory cells played little or no role in cholesterol homeostasis.

The HFD model did not induce a diabetic state by the 16 week endpoint with non-fasting glucose levels remaining below 200 mg/dL; however, the PAR2-KO mice demonstrated significantly lower mean plasma glucose compared to WT mice. Similar effects were shown in PAR2/tissue-factor-deficient mice, which was attributed in part to suppressing gluconeogenesis in liver [9,39]. Despite lower circulating glucose, glucose concentrations were actually slightly elevated in the livers of PAR2-KO mice compared to WT with significantly reduced pyruvate concentrations. This is consistent with suppression of hepatic glycolysis rather than gluconeogenesis in PAR2-deficient mice as reported previously [39]. The NMR-metabolomic data further indicated that excess hepatic glucose was directed instead to the alternate route of storage in the form of glycogen. Glycogen and its metabolites UDP-glucose and ascorbate were significantly elevated in the livers of the KO mice. Ascorbate (vitamin C) provides effective protection against ROS and circulating levels of vitamin C have been shown to be severely depleted in NAFLD subjects with metabolic syndrome [40]. Reactive oxygen species accumulate during maladaptive fatty acid breakdown in liver that has been ascribed to mitochondrial proton leakage in obese NASH patients [41]. The ascorbate reductant produced by elevated glycogen cycling may therefore provide substantial protection against β-oxidation-driven ROS damage and inflammation in the livers of the PAR2-deficient mice fed HFD. Indeed, previous studies showed that pharmacologic inhibition of PAR2 with a pepducin [8,42,43] protected against hepatocellular necrosis in NASH models and suppressed PAR2-induced ROS in hepatocytes [4].

Lastly, we investigated the underlying mechanism(s) by which PAR2 regulates hepatic lipid and cholesterol/bile steroid metabolism under conditions of HFD and identified G_i-Jnk1/2 as key downstream effectors of PAR2. Jnk is known to negatively regulate cholesterol catabolism in hepatocytes by inhibiting expression of the key bile acid synthesis enzyme Cyp7A1 in a SHP/FXR-dependent manner [20]. Increased hepatic Jnk activity ascribed to aberrant insulin signaling (non-GPCR) and inflammation/ROS has been described in the pathogenesis of NAFLD in NASH patients and mice [41]. There are varied explanations for the nexus between Jnk signaling and NAFLD. Jnk is reported to inhibit insulin signaling leading to peripheral and hepatic insulin resistance consequently promoting hepatic steatosis and gluconeogenesis in NAFLD [19,44]. Alternatively, Jnk1 can also regulate hepatic lipid metabolism in the absence of obesity and peripheral insulin resistance. TNFα and other inflammatory stimuli can activate AP-1/c-Jun nuclear signaling through Jnk [45] leading to bile steroid suppression [20]. In obese mice, Jnk1 can exert direct enhancing effects on sterol metabolism pathways in liver [46]. We found that protease activation of PAR2 leads to phosphorylation of Jnk1/2 via G_i coupling, which in turn upregulates the SREBP-1c lipogenic-regulatory transcription factor in hepatocytes. Accordingly, in PAR2-KO mice there is a reduction of active-SREBP-1c in liver, concordant with suppression of hepatic lipid anabolism and activation of phospho-AMPK. Lipid catabolism is induced in the PAR2-KO mouse livers with activation of AMPK targets PPARα, PGC-1α, PGC-1β, and a net decrease of hepatic triglyceride accumulation and steatosis.

5. CONCLUSIONS

In summary, we found that the protease-activated receptor PAR2 plays a critical role in regulating hepatic cholesterol and lipid metabolism in NAFLD. PAR2 expression levels increased in the livers of patients with more severe NAFLD fibrosis and higher plasma LDL cholesterol. Previous work had shown that LDL cholesterol levels can decrease with very severe fibrosis and cirrhosis [47]. Our findings that subjects with worse fibrosis have more PAR2 staining and higher PAR2 staining is associated with higher LDL cholesterol levels would appear to be counter to that trend. However, the earlier study excluded NASH subjects with diabetes and uncompensated cirrhosis, whereas 55% of our NAFLD and NASH subjects had diabetes, and our Fib 4 cohort included both compensated and uncompensated cirrhosis. As the blood samples were collected within 6 months of liver biopsy, this could add to variability in cholesterol and other lab values, though it is unlikely that fibrosis staging would appreciably change in that short time frame. Mechanistic studies identified G_i-Jnk1/2, SREBP-1c, and AMPK as key downstream effectors of protease-activated PAR2 metabolism in liver. This work adds to the precedence of protease-control of cholesterol and lipid homeostasis in liver (e.g. PCSK9-LDLR, SCAP-SREBP) under conditions of high-fat diet and fatty liver disease. The finding that PAR2 plays an important role in cholesterol homeostasis and hepatic lipid metabolism provides a rationale for the use of therapeutics to target this protease receptor in the setting of NAFLD and NASH and related metabolic conditions.

AUTHOR CONTRIBUTIONS

RR, AMS, NN, SG, and EKF performed experiments. RR, AMS, DHC, EKF, MA, YW, JB, LC, and AK designed the experiments and analyzed the data. RR and AK wrote the manuscript. RR, AMS, EKF, DHC, MA, JB, LC, and AK revised the manuscript. AK conceived the study.

ACKNOWLEDGEMENTS

We are grateful to Conor Calnan for initiating NMR metabolomic studies in mouse liver. This work was supported by a Post-doctoral Fellowship from the American Heart Association (RR), a Pre-doctoral F31 NRSA Fellowship from the NHLBI (AS), and by DK101240 (AK, LC) from the NIDDK and HL136485 from the NHLBI (AK), and NMR instrumentation NIH SIG grant S10OD020073.

CONFLICT OF INTEREST

LC and AK report serving as scientific founders of Oasis Pharmaceuticals.

APPENDIX A. SUPPLEMENTARY DATA

Supplementary data to this article can be found online at https://doi.org/10.1016/j.molmet.2019.08.019.

REFERENCES

[1] Samuel, V.T., Shulman, G.I., 2018. Nonalcoholic fatty liver disease as a nexus of metabolic and hepatic diseases. Cell Metabolism 27(1):22–41.

[2] Younossi, Z.M., 2018. Non-alcoholic fatty liver disease - a global public health perspective. Journal of Hepatology 70(3):531–544.

[3] Min, H.K., Kapoor, A., Fuchs, M., Mirshahi, F., Zhou, H., Maher, J., et al., 2012. Increased hepatic synthesis and dysregulation of cholesterol metabolism is associated with the severity of nonalcoholic fatty liver disease. Cell Metabolism 15(5):665–674.

[4] Shearer, A.M., Rana, R., Austin, K., Baleja, J.D., Nguyen, N., Bohm, A., et al., 2016. Targeting liver fibrosis with a cell-penetrating protease-activated receptor-2 (PAR2) pepducin. Journal of Biological Chemistry 291(44):23188–23198.

[5] Michael, E.S., Kuliopulos, A., Covic, L., Steer, M.L., Perides, G., 2013. Pharmacological inhibition of PAR2 with the pepducin P2pal-18S protects mice against acute experimental biliary pancreatitis. American Journal of Physiology Gastrointestinal and Liver Physiology 304(5):G516–G526.

[6] Sevigny, L.M., Austin, K.M., Zhang, P., Kasuda, S., Koukos, G., Sharifi, S., et al., 2011. Protease-activated receptor-2 modulates protease-activated receptor-1-driven neointimal hyperplasia. Arteriosclerosis Thrombosis and Vascular Biology 31(12):e100–e106.

[7] Kaneider, N.C., Leger, A.J., Agarwal, A., Nguyen, N., Perides, G., Derian, C., et al., 2007. 'Role reversal' for the receptor PAR1 in sepsis-induced vascular damage. Nature Immunology 8(12):1303–1312.

[8] Sevigny, L.M., Zhang, P., Bohm, A., Lazarides, K., Perides, G., Covic, L., et al., 2011. Interdicting protease-activated receptor-2-driven inflammation with cell-penetrating pepducins. Proceedings of the National Academy of Sciences of the United States of America 108(20):8491–8496.

[9] Badeanlou, L., Furlan-Freguia, C., Yang, G., Ruf, W., Samad, F., 2011. Tissue factor-protease-activated receptor 2 signaling promotes diet-induced obesity and adipose inflammation. Nature Medicine 17(11):1490–1497.

[10] Kleiner, D.E., Brunt, E.M., Van Natta, M., Behling, C., Contos, M.J., Cummings, O.W., et al., 2005. Design and validation of a histological scoring system for nonalcoholic fatty liver disease. Hepatology 41(6):1313–1321.

[11] Yu, C., Wang, F., Kan, M., Jin, C., Jones, R.B., Weinstein, M., et al., 2000. Elevated cholesterol metabolism and bile acid synthesis in mice lacking membrane tyrosine kinase receptor FGFR4. Journal of Biological Chemistry 275(20):15482–15489.

[12] Wu, H., Southam, A.D., Hines, A., Viant, M.R., 2008. High-throughput tissue extraction protocol for NMR- and MS-based metabolomics. Analytical Biochemistry 372(2):204–212.

[13] Dietschy, J.M., Turley, S.D., 2002. Control of cholesterol turnover in the mouse. Journal of Biological Chemistry 277(6):3801–3804.

[14] Shen, W.J., Azhar, S., Kraemer, F.B., 2018. SR-B1: a unique multifunctional receptor for cholesterol influx and efflux. Annual Review of Physiology 80:95–116.

[15] Pfeffer, S.R., 2019. NPC intracellular cholesterol transporter 1 (NPC1)-mediated cholesterol export from lysosomes. Journal of Biological Chemistry 294(5):1706–1709.

[16] Vila-Brau, A., De Sousa-Coelho, A.L., Mayordomo, C., Haro, D., Marrero, P.F., 2011. Human HMGCS2 regulates mitochondrial fatty acid oxidation and FGF21 expression in HepG2 cell line. Journal of Biological Chemistry 286(23):20423–20430.

[17] Inagaki, T., Dutchak, P., Zhao, G., Ding, X., Gautron, L., Parameswara, V., et al., 2007. Endocrine regulation of the fasting response by PPARalpha-mediated induction of fibroblast growth factor 21. Cell Metabolism 5(6):415–425.

[18] Badman, M.K., Pissios, P., Kennedy, A.R., Koukos, G., Flier, J.S., Maratos-Flier, E., 2007. Hepatic fibroblast growth factor 21 is regulated by PPARalpha and is a key mediator of hepatic lipid metabolism in ketotic states. Cell Metabolism 5(6):426–437.

[19] Czaja, M.J., 2010. JNK regulation of hepatic manifestations of the metabolic syndrome. Trends in Endocrinology and Metabolism 21(12):707–713.

[20] Gupta, S., Stravitz, R.T., Dent, P., Hylemon, P.B., 2001. Down-regulation of cholesterol 7alpha-hydroxylase (CYP7A1) gene expression by bile acids in primary rat hepatocytes is mediated by the c-Jun N-terminal kinase pathway. Journal of Biological Chemistry 276(19):15816–15822.

[21] Kalaany, N.Y., Mangelsdorf, D.J., 2006. LXRS and FXR: the yin and yang of cholesterol and fat metabolism. Annual Review of Physiology 68:159–191.

[22] Horton, J.D., Goldstein, J.L., Brown, M.S., 2002. SREBPs: activators of the complete program of cholesterol and fatty acid synthesis in the liver. Journal of Clinical Investigation 109(9):1125–1131.

[23] Li, Y., Xu, S., Mihaylova, M.M., Zheng, B., Hou, X., Jiang, B., et al., 2011. AMPK phosphorylates and inhibits SREBP activity to attenuate hepatic steatosis and atherosclerosis in diet-induced insulin-resistant mice. Cell Metabolism 13(4):376–388.

[24] Barr, T.P., Garzia, C., Guha, S., Fletcher, E.K., Nguyen, N., Wieschhaus, A.J., et al., 2019. PAR2 pepducin-based suppression of inflammation and itch in atopic dermatitis models. Journal of Investigative Dermatology 139(2):412–421.

[25] Michael, E.S., Covic, L., Kuliopulos, A., 2019. Trace amine-associated receptor 1 (TAAR1) promotes anti-diabetic signaling in insulin-secreting cells. Journal of Biological Chemistry 294(12):4401–4411.

[26] Phillips, M.C., 2014. Molecular mechanisms of cellular cholesterol efflux. Journal of Biological Chemistry 289(35):24020–24029.

[27] Jones, S.M., Mann, A., Conrad, K., Saum, K., Hall, D.E., McKinney, L.M., et al., 2019. PAR2 (Protease-Activated receptor 2) deficiency attenuates atherosclerosis in mice. Arteriosclerosis Thrombosis and Vascular Biology 38(6):1271–1282.

[28] Neumann, J., Rose-Sperling, D., Hellmich, U.A., 2017. Diverse relations between ABC transporters and lipids: an overview. Biochimica et Biophysica Acta Biomembranes 1859(4):605–618.

[29] Okushin, K., Tsutsumi, T., Enooku, K., Fujinaga, H., Kado, A., Shibahara, J., et al., 2016. The intrahepatic expression levels of bile acid transporters are inversely correlated with the histological progression of nonalcoholic fatty liver disease. Journal of Gastroenterology 51(8):808–818.

[30] Donnelly, K.L., Smith, C.I., Schwarzenberg, S.J., Jessurun, J., Boldt, M.D., Parks, E.J., 2005. Sources of fatty acids stored in liver and secreted via lipoproteins in patients with nonalcoholic fatty liver disease. Journal of Clinical Investigation 115(5):1343–1351.

[31] Kim, C.W., Addy, C., Kusunoki, J., Anderson, N.N., Deja, S., Fu, X., et al., 2017. Acetyl CoA carboxylase inhibition reduces hepatic steatosis but elevates plasma triglycerides in mice and humans: a bedside to bench investigation. Cell Metabolism 26(3):394–406.

[32] Mar-Heyming, R., Miyazaki, M., Weissglas-Volkov, D., Kolaitis, N.A., Sadaat, N., Plaisier, C., et al., 2008. Association of stearoyl-CoA desaturase 1 activity with familial combined hyperlipidemia. Arteriosclerosis Thrombosis and Vascular Biology 28(6):1193–1199.

[33] Puchalska, P., Crawford, P.A., 2017. Multi-dimensional roles of ketone bodies in fuel metabolism, signaling, and therapeutics. Cell Metabolism 25(2):262–284.

[34] Kersten, S., Seydoux, J., Peters, J.M., Gonzalez, F.J., Desvergne, B., Wahli, W., 1999. Peroxisome proliferator-activated receptor alpha mediates the adaptive response to fasting. Journal of Clinical Investigation 103(11):1489–1498.

[35] Hashimoto, T., Cook, W.S., Qi, C., Yeldandi, A.V., Reddy, J.K., Rao, M.S., 2000. Defect in peroxisome proliferator-activated receptor alpha-inducible fatty acid oxidation determines the severity of hepatic steatosis in response to fasting. Journal of Biological Chemistry 275(37):28918–28928.

[36] Le May, C., Pineau, T., Bigot, K., Kohl, C., Girard, J., Pegorier, J.P., 2000. Reduced hepatic fatty acid oxidation in fasting PPARalpha null mice is due to impaired mitochondrial hydroxymethylglutaryl-CoA synthase gene expression. FEBS Letters 475(3):163–166.

[37] Rui, L., 2014. Energy metabolism in the liver. Comparative Physiology 4(1): 177–197.

[38] McGarry, J.D., Mannaerts, G.P., Foster, D.W., 1977. A possible role for malonyl-CoA in the regulation of hepatic fatty acid oxidation and ketogenesis. Journal of Clinical Investigation 60(1):265–270.

[39] Wang, J., Chakrabarty, S., Bui, Q., Ruf, W., Samad, F., 2015. Hematopoietic tissue factor-protease-activated receptor 2 signaling promotes hepatic inflammation and contributes to pathways of gluconeogenesis and steatosis in obese mice. American Journal Of Pathology 185(2):524–535.

[40] Palmieri, V.O., Grattagliano, I., Portincasa, P., Palasciano, G., 2006. Systemic oxidative alterations are associated with visceral adiposity and liver steatosis in patients with metabolic syndrome. Journal of Nutrition 136(12):3022–3026.

[41] Koliaki, C., Szendroedi, J., Kaul, K., Jelenik, T., Nowotny, P., Jankowiak, F., et al., 2015. Adaptation of hepatic mitochondrial function in humans with non-alcoholic fatty liver is lost in steatohepatitis. Cell Metabolism 21(5):739–746.

[42] Covic, L., Gresser, A.L., Talavera, J., Swift, S., Kuliopulos, A., 2002. Activation and inhibition of G protein-coupled receptors by cell-penetrating membrane-tethered peptides. Proceedings of the National Academy of Sciences of the United States of America 99(2):643–648.

[43] Miller, J., Agarwal, A., Devi, L.A., Fontanini, K., Hamilton, J.A., Pin, J.P., et al., 2009. Insider access: pepducin symposium explores a new approach to GPCR modulation. Annals of the New York Academy of Sciences 1180(Suppl. 1):E1–E12.

[44] Nakatani, Y., Kaneto, H., Kawamori, D., Hatazaki, M., Miyatsuka, T., Matsuoka, T.A., et al., 2004. Modulation of the JNK pathway in liver affects insulin resistance status. Journal of Biological Chemistry 279(44):45803–45809.

[45] Rana, R., Huang, T., Koukos, G., Fletcher, E.K., Turner, S.E., Shearer, A., et al., 2018. Noncanonical matrix metalloprotease 1-protease-activated receptor 1 signaling drives progression of atherosclerosis. Arteriosclerosis Thrombosis and Vascular Biology 38(6):1368–1380.

[46] Yu, X.X., Murray, S.F., Watts, L., Booten, S.L., Tokorcheck, J., Monia, B.P., et al., 2008. Reduction of JNK1 expression with antisense oligonucleotide improves adiposity in obese mice. American Journal of Physiology Endocrinology and Metabolism 295(2):E436–E445.

[47] Siddiqui, M.S., Fuchs, M., Idowu, M.O., Luketic, V.A., Boyett, S., Sargeant, C., et al., 2015. Severity of nonalcoholic fatty liver disease and progression to cirrhosis are associated with atherogenic lipoprotein profile. Clinical Gastroenterology and Hepatology 13(5):1000–1008 e1003.

